Article

Simulation of Gold Nanoparticle Transport during MHD Electroosmotic Flow in a Peristaltic Micro-Channel for Biomedical Treatment

Muneerah Al Nuwairan [1] (ID) **and Basma Souayeh** [2,3,*] (ID)

1 Department of Mathematics and Statistics, College of Science, King Faisal University, P.O. Box 400, Al-Ahsa 31982, Saudi Arabia; msalnuwairan@kfu.edu.sa
2 Department of Physics, College of Science, King Faisal University, P.O. Box 400, Al-Ahsa 31982, Saudi Arabia
3 Laboratory of Fluid Mechanics, Physics Department, Faculty of Sciences of Tunis, University of Tunis El Manar, 2092 Tunis, Tunisia
* Correspondence: bsouayeh@kfu.edu.sa or basma.souayeh@gmail.com

Abstract: The study of gold nanoparticles (AuNPs) in the blood flow has emerged as an area of interest for numerous researchers, due to its many biomedical applications, such as cancer radiotherapy, DNA and antigens, drug and gene delivery, in vitro evaluation, optical bioimaging, radio sensitization and laser phototherapy of cancer cells and tumors. Gold nanoparticles can be amalgamated in various shapes and sizes. Due to this reason, gold nanoparticles can be diffused efficiently, target the diseased cells and destroy them. The current work studies the effect of gold nanoparticles of different shapes on the electro-magneto-hydrodynamic (EMHD) peristaltic propulsion of blood in a micro-channel under various effects, such as activation energy, bioconvection, radiation and gyrotactic microorganisms. Four kinds of nanoparticle shapes, namely bricks, cylinders and platelets, are considered. The governing equations are simplified under the approximations of low Reynolds number (LRN), long wavelength (LWL) and Debye–Hückel linearization (DHL). The numerical solutions for the non-dimensional equations are solved using the computational software MATLAB with the help of the bvp4c function. The influences of different physical parameters on the flow and thermal characteristics are computed through pictorial interpretations.

Keywords: bioconvection; activation energy; gyrotactic microorganisms; gold nanoparticles; physiological flow; electroosmosis

1. Introduction

Recent developments in nanotechnology have motivated the creation of various nanoparticles [1–4]. Among the existing nanoparticles, metallic nanoparticles have been used widely in biomedical treatments and, among them, AuNPs attract extreme attention, due to their inherent characteristics, such as surface plasmon resonance (SPR), and their physicochemical, electronic and optical fields, which can be easily modified by converting the particle characterizations, such as environment, aspect ratio, size and shape. This leads to the provision of extreme functionalization properties, of use in many applications in diverse categories of biomedicine, for instance, in imaging, targeted drug delivery, sensing, bioimaging, photodynamic and photothermal therapy. Gold nanoparticles have been greatly used for diagnostics of disease, therapeutics [5], tumor necrosis factor, transmission electron microscopy, scanning electron microscopy, polyethylenglycol and plasmonic photothermal therapy [6]. In the last few decades, many researchers have shown the various applications of gold nanoparticles in diverse areas. For instance, Elahi et al. [7] provided a short review on the various applications of gold nanoparticles. In their study, they have concluded that gold nanoparticles have many applications in biomedicine, such as oncological diseases, certain skin or infectious diseases, hyperthermia, X-ray imaging and photoacoustic imaging. Daraee et al. [8] proved the AuNPs can play an excellent role in solving the

problems of bioimaging (optical coherence tomography, confocal laser microscopy and resonance scattering dark-field microscopy). Bansal et al. [9] provided a review on the achievements in and the importance of AuNPs in the biomedical field. AuNPs are widely used in nanoelectronics, as has been shown by Homberger and Simon [10]. In light of the aforementioned reviews and experimental works, more recently, investigators have started working on nanofluid flows suspended by gold nanoparticles from a biological point of view. Mekheimer et al. [11] provided a theoretical study on the peristaltic propulsion of blood flow with gold nanoparticles as a third-grade nanofluid in a catheter, which is applicable in cancer therapy. Koriko et al. [12] presented MATLAB bvp4c solutions for the blood–gold Carreau nanoliquid flow. Ellahi et al. [13] used the homotopy perturbation method to study the blood flow of a nanofluid in composite stenosed arteries. Riaz et al. [14] studied the Jeffrey nanofluid flow in two eccentric asymmetric annuli with the help of the homotopy perturbation method. Elnaqeeb et al. [15] discussed the propulsion of gold nanoparticles in the blood in overlapped stenosis.

It is well known that the magnetic field can be used to treat various diseases. The Arabian physician Avicenna used magnets to treat diseases of the liver in about 1000 A.D. The Persian physician Abbas wrote a book named "Perfect Book of the Art of Medicine" and claimed that magnetism can cure gout and spasms. Later, the Swiss physician Paracelsus used magnets to treat hernias, dropsy and jaundice [16]. Magnetic fields can cure many ailments and is used in the hyperthermia treatment of cancer, as an MRI contrast agent, drug delivery method, in magnetic bio-separation and nervous disorders [17]. Roth [18] provided a review on the applications of magnetic forces in medicine, such as magnetic resonance imaging, magneto-acoustic tomography, Hall effect imaging and magneto-acoustic imaging. Zablotskii et al. [19] proved that magnetic fields affect cell life and discussed their many applications in targeted stem cell delivery, cell therapy, cell biology, and nanomedicine. In view of the aforementioned applications, many researchers have started working on magnetic fields towards the achievement of physiological vessels. Eldabe et al. [20] used the differential transform method to investigate the MHD Carreau nanofluid flow in a peristaltic channel suspended by gold nanoparticles, which was useful in destroying cancer cells. Abdelsalam and Bhatti [21] provided the analytical results of the MHD peristaltic nanofluid flow with suspended gold nanoparticles and concluded that their findings may be useful in in eradicating tumor cells. Akram et al. [22] obtained the exact solutions for the nanofluid flow through a peristaltic channel under a uniform magnetic field. El-Dabe et al. [23] utilized a numerical technique, named the Runge–Kutta–Merson method, to discuss the motion of a nanofluid during inclined peristalsis. Devaki et al. [24] discussed the MHD nanofluid flow in an artery with mild stenosis and concluded that their findings may be helpful in destroying of the stencils. Reddy and Makinde [25] used the Runge–Kutta–Fehlberg method to depict the results of MHD Jeffrey nanofluid motion in an asymmetric channel.

In the last few decades, the level of electromagnetic fields (EMFs) of natural and man-made origin has continuously increased, due to their wide variety of applications in diverse research fields, such as wound healing, cartilage/bone repair, pain control, inhabitation of cancer growth, plastic surgery, electro-chemotherapy, gene therapy, non-thermal ablation, tendon injuries [26]. Ryan et al. [27] provided an experimental study on electric field simulation for tissue engineering applications. Cen and Chen [28] presented electric field applications found in pulsed electric field treatments in vitro and in vivo. There are other applications that have been shown in transcranial magnetic stimulation and nerve electrophysiology with respect to electric and magnetic fields [29]. Moatimid et al. [30] discussed the influences of electroosmosis on nanofluid flow in a peristaltic micro-channel and that are useful in cancer therapy. Tanveer et al. [31] presented a theoretical investigation on the motion of a nanofluid under electroosmosis and peristalsis. Sharma et al. [32] provided analytical solutions for nanofluid flow in a fluidic peristaltic channel with electroosmosis and their findings can be useful in particle filtrations and cell therapeutics. Prakash et al. [33] studied the motion of a tangent hyperbolic nanofluid via peristaltic pump-

ing with electroosmosis effects with the help of the perturbation method. Noreen et al. [34] discussed the flow of an EMHD nanofluid in an asymmetric microfluidic channel. Mekheimer et al. [35] used gold nanoparticles in a base fluid to discuss the flow characteristics in an EMHD peristaltic channel.

Motivated by the aforementioned investigations, the effect of electroosmosis, magnetic field, activation energy, bioconvection and radiation on the gold–blood nanofluid flow in an asymmetric peristaltic channel is considered in the current article. The different shapes of nanoparticles are considered in the present model since the nanoparticles show characteristic colors and properties with variations in size and shape, which can be utilized in cutting-edge materials, biological imaging and biomedicine [36]. The governing equations are simplified under the lubrication approach and Debye–Hückel linearization process. The resulting highly non-linear system of differential equations area solved numerically under the mathematical computational scheme MATLAB bvp4c. The pictorial representations for the velocity, temperature, nanoparticle volume fraction, shear stress and microorganism concentration are presented for sundry parameters.

2. Mathematical Model

2.1. Problem Formulation

Peristalsis is a contraction and relaxation of muscles that propagates in a wave down a channel/tube. This kind of situation can be seen in many physiological situations, such as food flow through the esophagus, bile flow through the bile duct and intrauterine fluid motions. For example, in the digestive tract, peristalsis starts in the esophagus where strong wave-like motions of the smooth muscle move balls of swallowed food to the stomach. There, the food is churned into a liquid mixture called chyme that moves into the small intestine where peristalsis continues. We considered the mathematical modeling of EMHD gold–blood nanofluid flow in a peristaltic asymmetric vessel. The influence of bioconvection, activation energy, thermal radiation, and the different shapes of nanoparticles, such as bricks, platelets and cylinders, were taken into account. The Cartesian (X, Y) system is assumed transverse and parallel to the path of wave propagation. The motion is assumed under the electroosmosis and peristalsis behavior. The uniform magnetic field B_0 is applied in the transverse direction of the actual fluid motion. It is also assumed that the left wall of the peristalsis was maintained at temperature, concentrations and motile organisms as T_0, C_0, N_0. The temperature, concentrations and motile organisms of right peristalsis wall were considered as T_1, C_1, N_1 (see Figure 1). The geometries of the left and right peristalsis walls were represented as [37]

$$H_1(X, t) = -d - a_1 \cos^2\left(\frac{\pi}{\lambda}(X - ct) + \phi\right), \tag{1}$$

$$H_2(X, t) = d + a_2 \cos^2\left(\frac{\pi}{\lambda}(X - ct)\right), \tag{2}$$

where H_1 is the left peristaltic wall, H_2 is the right peristaltic wall, d denotes the width of the channel, a_1 represents wave amplitude of left wall, a_2 is the wave amplitude of right wall, λ denotes the wavelength, t is the time, c is the wave speed and ϕ represents phase difference; for $\phi = 0$, the corresponding problem is converted to symmetric model.

The governing equations (continuity, momentum, energy, nanoparticle volume fraction and microorganisms) for the nanofluid flow in the fixed frame are expressed as [38–40].

$$\frac{\partial U}{\partial X} + \frac{\partial V}{\partial Y} = 0, \tag{3}$$

$$\rho_{nf}\left(\frac{\partial U}{\partial t} + U\frac{\partial U}{\partial X} + V\frac{\partial U}{\partial Y}\right) = -\frac{\partial P}{\partial X} + \mu_{nf}\left(\frac{\partial^2 U}{\partial X^2} + \frac{\partial^2 U}{\partial Y^2}\right) - \sigma_{nf}B_0{}^2 U + \rho_e E_x$$
$$+ (\rho\beta)_{nf}g(1 - C_0)(T - T_0) - g(\rho_p - \rho_f)(C - C_0) - g\gamma(\rho_m - \rho_f)(N - N_0), \tag{4}$$
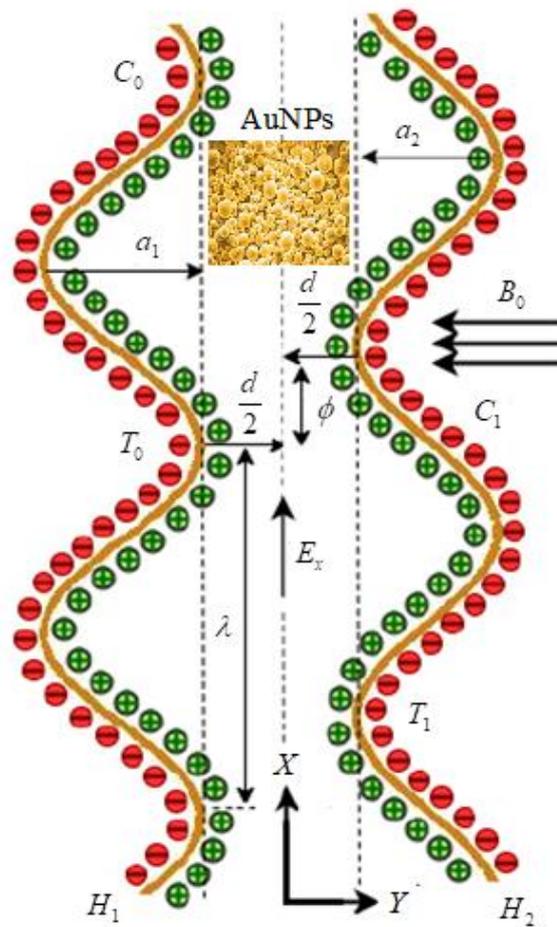
Figure 1. Schematic flow representation in the presence of EMHD and gold nanoparticles.

$$\rho_{nf}\left(\frac{\partial V}{\partial t} + U\frac{\partial V}{\partial X} + V\frac{\partial V}{\partial Y}\right) = -\frac{\partial P}{\partial Y} + \mu_{nf}\left(\frac{\partial^2 V}{\partial X^2} + \frac{\partial^2 V}{\partial Y^2}\right),$$ (5)

$$(\rho c_p)_{nf}\left(\frac{\partial T}{\partial t} + U\frac{\partial T}{\partial X} + V\frac{\partial T}{\partial Y}\right) = \left(k_{nf} + \frac{16\sigma^* T_0^3}{3k^*}\right)\left(\frac{\partial^2 T}{\partial X^2} + \frac{\partial^2 T}{\partial Y^2}\right)$$
$$+ (\rho c_p)_p\left(D_B\left(\frac{\partial C}{\partial X}\frac{\partial T}{\partial X} + \frac{\partial C}{\partial Y}\frac{\partial T}{\partial Y}\right) + \frac{D_T}{T_m}\left(\left(\frac{\partial T}{\partial X}\right)^2 + \left(\frac{\partial T}{\partial Y}\right)^2\right)\right),$$ (6)

$$\frac{\partial C}{\partial t} + U\frac{\partial C}{\partial X} + V\frac{\partial C}{\partial Y} = D_B\left(\frac{\partial^2 C}{\partial X^2} + \frac{\partial^2 C}{\partial Y^2}\right) + \frac{D_T}{T_m}\left(\frac{\partial^2 T}{\partial X^2} + \frac{\partial^2 T}{\partial Y^2}\right) - k_r^2(C - C_0)\left(\frac{T}{T_0}\right)^n \exp\left(\frac{-E_a}{\omega T}\right),$$ (7)

$$\frac{\partial N}{\partial t} + U\frac{\partial N}{\partial X} + V\frac{\partial N}{\partial Y} + \frac{b^* W_e}{(C_1 - C_0)}\left(\frac{\partial}{\partial X}\left(N\frac{\partial C}{\partial X}\right) + \frac{\partial}{\partial Y}\left(N\frac{\partial C}{\partial Y}\right)\right) = D_m\left(\frac{\partial^2 N}{\partial X^2} + \frac{\partial^2 N}{\partial Y^2}\right),$$ (8)

with the corresponding boundary conditions [41–43]:

$$U = 0, \psi = -\frac{F}{2}, T = T_0, C = C_0, N = N_0 \text{ at } Y = H_1\left(= -d - a_1\cos^2\left(\frac{\pi}{\lambda}(X - ct) + \phi\right)\right),$$ (9)

$$U = 0, \psi = \frac{F}{2}, T = T_1, C = C_1, N = N_1 \text{ at } Y = H_2\left(= d + a_2\cos^2\left(\frac{\pi}{\lambda}(X - ct)\right)\right),$$ (10)

where U, V denote the velocities in X and Y directions, respectively; ρ_{nf} is nanofluid effective density; t is time; μ_{nf} is the nanofluid dynamic viscosity; σ_{nf} is the nanofluid electrical conductivity; $(\rho\beta)_{nf}$ is the effective thermal expansion; g is the gravitational force; T is the nanoparticle temperature; ρ_p is density of nanoparticle; ρ_f is density of the base fluid; N is motile density; N_0 is ambient concentration of motile organisms; γ is volume of microorganisms; ρ_m is motile organisms density; ρ_e is electrical charge density; E_x is applied electric field; $(\rho c_p)_{nf}$ is effective heat capacity of nanofluid; k_{nf} is thermal diffusivity of nanofluid; σ^* is the Stefan–Boltzmann constant; k^* is mean absorption coefficient; D_B is Brownian diffusion coefficient; C is nanoparticle concentration; D_T is thermophoretic diffusion coefficient; T_m is mean temperature; k_r is the rate of reaction; n is the fitted rate $(-1 < n < 1)$; E_a is activation energy; ω is the Boltzmann constant $(8.61 \times 10^{-5} ev/K)$; b^* is chemotaxis constant; W_e is swimming cells speed; P is pressure; ψ is the dimensional stream function; F is the dimensional constant flow rate; and D_m is the microorganism diffusion coefficient. In Equation (6), the radiation effects were considered under the Rosseland approximation and simplified with the help of Taylor's series expansion.

2.2. Electrohydrodynamics

In a micro-channel, the Poisson equation is defined [44] as:

$$\nabla^2 \overline{\varphi} = -\frac{\rho_e}{\xi},\tag{11}$$

where $\overline{\varphi}$ denotes the electric potential, ξ is the dielectric permittivity, and ρ_e represents the total charge density.

The net charge density ρ_e follows the Boltzmann variation [45] and is

$$\rho_e = -z_v e\left(\overline{n}^- - \overline{n}^+\right).\tag{12}$$

The anions $(\overline{n}^-)$ and captions $(\overline{}\overline{n}^+)$ are distinct by ρ_e of the Boltzmann equation:

$$\overline{n}^\pm = n_0 e^{\left(\pm\frac{e z_v}{T_{av} K_B}\overline{\varphi}\right)},\tag{13}$$

where, n_0 denotes bulk concentration, K_B the Boltzmann constant, z_v the charge balance, e the electronic charge and T_{av} is the average temperature. Employing Debye–Hückel linearization estimation [45], Equation (11) revolves to

$$\frac{d^2\varphi}{dy^2} = \kappa^2 \varphi,\tag{14}$$

where κ represents the electroosmotic expression. The analytical solution of Equation (14) with boundary conditions (BCs): $\varphi = \zeta_1$ at $y = h_1$ and $\varphi = \zeta_2$ at $y = h_2$ was reached as:

$$\varphi = \left(\frac{\varsigma_2\sinh(\kappa h_1) - \varsigma_1\sinh(\kappa h_2)}{\sinh(\kappa(h_1 - h_2))}\right)\cosh(\kappa y) - \left(\frac{\varsigma_2\cosh(\kappa h_1) - \varsigma_1\cosh(\kappa h_2)}{\sinh(\kappa(h_1 - h_2))}\right)\sinh(\kappa y).\tag{15}$$

2.3. Thermophysical Properties and Geometries of Nanoparticles

The thermophysical characteristics of gold blood nanofluid are given in Table 1, and are expressed via equations as follow [41,46,47]:

$$\rho_{nf} = \rho_f\left((1 - \varphi_1) + \varphi_1\left(\frac{\rho_p}{\rho_s}\right)\right),\tag{16}$$

$$(\rho\beta)_{nf} = (\rho\beta)_f\left((1 - \varphi_1) + \varphi_1\left(\frac{(\rho\beta)_p}{(\rho\beta)_f}\right)\right),\tag{17}$$

$$(\rho c_p)_{nf} = (\rho c_p)_f \left((1 - \varphi_1) + \varphi_1 \left(\frac{(\rho c_p)_p}{(\rho c_p)_f} \right) \right), \tag{18}$$

$$\mu_{nf} = \mu_f \left(1 + A_1 \varphi_1 + A_2 \varphi_1^2 \right), \tag{19}$$

$$k_{nf} = k_f \left(\frac{k_p + (s-1)k_f - (s-1)\varphi_1 \left(k_f - k_p \right)}{k_p + (s-1)k_f + \varphi_1 \left(k_f - k_p \right)} \right), \tag{20}$$

$$\sigma_{nf} = \sigma_f \left(1 + \frac{3 \left(\frac{\sigma_p}{\sigma_f} - 1 \right) \varphi_1}{\left(\frac{\sigma_p}{\sigma_f} + 2 \right) - \left(\frac{\sigma_p}{\sigma_f} - 1 \right) \varphi_1} \right), \tag{21}$$

Table 1. Thermophysical properties of gold nanoparticles and base fluid (blood) [43,47].

Properties	Gold	Blood
$k(W/mK)$	314	0.492
$c_p(J/kgK)$	129	3594
$\rho(kg/m^3)$	19,320	1063
$\sigma(S/m)$	4.52×10^7	0.667
$\beta(1/k) \times 10^{-5}$	1.4	0.18
$(kg/m.s)$	-	0.0004
Pr	-	21

2.4. Non-Dimensional Governing Equations and Boundary Conditions

We introduce the transformations between the wave and fixed frame:

$$x = X - ct, \;\; y = Y, \;\; u = U - c, \;\; v = V, \;\; p = P, \overline{N} = N, \;\; \overline{T} = T, \overline{C} = C. \tag{22}$$

Additionally, the non-dimensional quantities were:

$$\overline{u} = \frac{u}{c}, \overline{v} = \frac{v}{c\delta}, \overline{x} = \frac{x}{\lambda}, \overline{y} = \frac{y}{d}, \overline{p} = \frac{d^2 p}{c\lambda\mu_f}, \theta = \frac{\overline{T} - T_0}{T_1 - T_0}, \sigma = \frac{\overline{C} - C_0}{C_1 - C_0}, \chi = \frac{\overline{N} - N_0}{N_1 - N_0},$$

$$M = \sqrt{\frac{\sigma_f}{\mu_f}} B_0 d, \text{Re} = \frac{\rho_f cd}{\mu_f}, \delta = \frac{d}{\lambda}, Rb = \frac{(\rho_m - \rho_f)\gamma(N_1 - N_0)}{(\rho\beta)_f (1 - C_0)(T_1 - T_0)},$$

$$Gr = \frac{g(\rho\beta)_f (1 - C_0)(T_1 - T_0)d^2}{c\mu_f}, Nr = \frac{(\rho_m - \rho_f)(C_1 - C_0)}{(\rho\beta)_f (1 - C_0)(T_1 - T_0)}, Rn = \frac{16\sigma^* T_0^3}{3k^* \mu_f (c_p)_f}, \tag{23}$$

$$\tau = \frac{(\rho c_p)_p}{(\rho c_p)_f}, \text{Pr} = \frac{\mu_f (c_p)_f}{k_f}, \xi = \frac{k_r^2 d^2}{\mu_f}, Sc = \frac{\mu_f}{\rho_f D_B}, \beta = \frac{T_1 - T_0}{T_0}, E = \frac{E_a}{\omega T_0},$$

$$Nb = \frac{\rho_f \tau D_B (C_1 - C_0)}{\mu_f}, Nt = \frac{\rho_f \tau D_T (T_1 - T_0)}{\mu_f T_m}, Pe = \frac{b_1^* W_e}{D_m}, \Omega = \frac{N_0}{N_1 - N_0},$$

$$U_{HS} = -\frac{E_x \varepsilon_{ef} \zeta_1}{c\mu_f}, \kappa = dez \sqrt{\frac{2n_0}{\varepsilon_{ef} k_B T_e}}, u = \frac{\partial \psi}{\partial y}, v = -\delta \frac{\partial \psi}{\partial x}, \overline{\psi} = \frac{\psi}{ca_1}, \overline{F} = \frac{F}{cd}.$$

The analysis was carried out under the assumption that the width of the channel is small compared to the wavelength of peristaltic waves. This assumption is usually called long wavelength approximation. Such consideration is realistic when peristalsis for ureter, chyme movement in intestine and spermatozoa in ductus efferences are considered. The Reynolds number was taken low. The long wavelength and low Reynolds number approximations are used extensively in the analysis of peristaltic flows. It should be pointed out that the theory of long wavelength and zero Reynolds number remains applicable for case of chyme transport in small intestine [48].

Using the aforementioned theory, and assumptions (long wavelength and low Reynolds number), the appropriate non-dimensional governing equations (in wave frame) are written as:

$$\frac{\mu_{nf}}{\mu_f}\frac{\partial^4\psi}{\partial y^4} - \frac{\sigma_{nf}}{\sigma_f}M^2\frac{\partial^2\psi}{\partial y^2} + Gr\left(\frac{(\rho\beta)_{nf}}{(\rho\beta)_f}\frac{\partial\theta}{\partial y} - Nr\frac{\partial\sigma}{\partial y} - Rb\frac{\partial\chi}{\partial y}\right)$$
$$+\kappa^3 U_{HS}\left(\left(\frac{\varsigma_2\sinh(\kappa h_1)-\varsigma_1\sinh(\kappa h_2)}{\sinh(\kappa(h_1-h_2))}\right)\sinh(\kappa y) - \left(\frac{\varsigma_2\cosh(\kappa h_1)-\varsigma_1\cosh(\kappa h_2)}{\sinh(\kappa(h_1-h_2))}\right)\cosh(\kappa y)\right) = 0, \quad (24)$$

$$\left(\frac{k_{nf}}{k_f} + RnPr\right)\frac{\partial^2\theta}{\partial y^2} + Nb\,Pr\frac{\partial\theta}{\partial y}\frac{\partial\sigma}{\partial y} + Nt\,Pr\left(\frac{\partial\theta}{\partial y}\right)^2 = 0, \quad (25)$$

$$\frac{\partial^2\sigma}{\partial y^2} + \frac{Nt}{Nb}\frac{\partial^2\theta}{\partial y^2} - Sc\xi\sigma(1+\beta\theta)^n\exp\left(-\frac{E}{1+\beta\theta}\right) = 0, \quad (26)$$

$$\frac{\partial^2\chi}{\partial y^2} - Pe(\chi+\Omega)\frac{\partial^2\sigma}{\partial y^2} - Pe\frac{\partial\chi}{\partial y}\frac{\partial\sigma}{\partial y} = 0, \quad (27)$$

with the corresponding dimensionless boundary conditions

$$\psi = -\frac{F}{2},\ \frac{\partial\psi}{\partial y} = -1,\ \theta = 0, \sigma = 0,\ \chi = 0\ \text{at}\ y = h_1\left(= -1 - a\cos^2(\pi x + \phi)\right), \quad (28)$$

$$\psi = \frac{F}{2},\ \frac{\partial\psi}{\partial y} = -1,\ \theta = 1,\ \sigma = 1,\ \chi = 1\ \text{at}\ y = h_2\left(= 1 + b\cos^2(\pi x)\right), \quad (29)$$

where $Q(= F + 2 + (a+b)/2)$ is the time mean flow rate in the fixed frame and $F = \int_{h_1}^{h_2}(\partial\psi/\partial y)dy$ is the time mean flow rate in the wave frame.

In the above expressions, θ is nanoparticle temperature; σ is nanoparticle concentration; χ is motile microorganisms; M is Hartmann number; Re is the Reynolds number; δ is the wave number; Rb is the bioconvection Rayleigh constant; Gr is the thermal Grashof number; Nr is the buoyancy ratio constant; Rn is the radiation parameter; τ is the effective heat capacity ratio of nanoparticle material-to-liquid heat capacity; Pr is the Prandtl number; ξ is the reaction rate constant; Sc is the Schmidt number; β is the temperature ratio parameter; E is the activation energy parameter; Nb is the Brownian motion parameter; Nt is the thermophoresis parameter; Pe is the Peclet number; Ω is the concentration difference constant for the microorganisms; U_{HS} is the Helmholtz–Smoluchowski velocity; κ is the electroosmosis parameter; ς_1 and ς_2 are the zeta potentials; F is the volume flow rate in the wave frame; and ψ is stream function.

The standard non-dimensional shear stress at the left wall can be represented as

$$\tau_s = \frac{\mu_{nf}}{\mu_f}\left(\frac{\partial u}{\partial y}\right)_{y=h_1}. \quad (30)$$

3. Numerical Procedure

The numerical solution of Equations (24)–(27) along with (28)–(29) can be represented with bvp4c scheme. The mechanism behind bvp4c MATLAB software is the finite difference method. The system of higher order differential equations is renovated into an ordinary differential equation, representing $\psi = y_1$, $\psi' = y_2$, $\psi'' = y_3$, $\psi''' = y_4$, $\theta = y_5$, $\theta' = y_6$, $\sigma = y_7$, $\sigma' = y_8$, $\chi = y_9$, $\chi' = y_{10}$. Thus Equations (24)–(29) can be expressed as

$$y_1' = y_2,$$
$$y_2' = y_3,$$
$$y_3' = y_4,$$
$$y_4' = \frac{1}{a_1}\left(\begin{array}{l} a_2 M^2 y_3 - Gr(a_3 y_6 - Nry_8 - Rby_{10}) \\ -\kappa^3 U_{HS}\left(\left(\dfrac{\varsigma_2 \sinh(\kappa h_1) - \varsigma_1 \sinh(\kappa h_2)}{\sinh(\kappa(h_1 - h_2))}\right)\sinh(\kappa y) - \left(\dfrac{\varsigma_2 \cosh(\kappa h_1) - \varsigma_1 \cosh(\kappa h_2)}{\sinh(\kappa(h_1 - h_2))}\right)\cosh(\kappa y)\right) \end{array} \right),$$
$$y_5' = y_6,$$
$$y_6' = \frac{-1}{a_4 + RnPr}\left(NbPr y_6 y_8 + NtPr(y_6)^2\right)$$
$$y_7' = y_8,$$
$$y_8' = -\frac{Nt}{Nb}y_6' + Sc\xi y_7(1 + \beta y_5)^n \exp\left(-\frac{E}{1 + \beta y_5}\right),$$
$$y_9' = y_{10},$$
$$y_{10}' = Pe(\chi + \Omega)y_8' + Pe y_8 y_{10}$$

$$(31)$$

with the following boundary conditions:

$$y_1(h_1) = -\tfrac{F}{2},\ y_2(h_1) = -1,\ y_5(h_1) = 0,\ y_7(h_1) = 0,\ y_9(h_1) = 0;$$
$$y_1(h_2) = \tfrac{F}{2},\ y_2(h_2) = -1,\ y_5(h_2) = 1,\ y_7(h_2) = 1,\ y_9(h_2) = 1.$$

$$(32)$$

4. Results and Discussion

In the current section, pictorial representations are presented for the velocity u, temperature θ, nanoparticle volume fraction σ, microorganisms χ, shear stress τ_s and Nusselt number Nu for the various parameters with various ranges, such as the Hartmann number M (range 0–6); thermal Grashof number M (range 0–6); Helmholtz–Smoluchowski velocity U_{HS} (range -3–9); shape factor s (nanoparticle shapes are provided in Figure 2, and the values of the shape factors can be found in Table 2); radiation parameter Rn (range 0.1–0.7); thermophoresis parameter Nt (range 1–9); Brownian motion parameter Nb (range 0.1–0.9); activation energy parameter E (range 1–4); temperature ratio parameter β (range 0–3); Peclet number Pe (range 0–0.9); electroosmosis parameter κ (range 2–2.3); zeta potential ς_1(range 1–1.6); bioconvection Rayleigh constant Rb (range 1–1.6) and buoyancy ratio constant Nr (range 1–1.6). Figure 3 presents the influences of various parameters, such as the Hartmann number M, thermal Grashof number Gr, Helmholtz–Smoluchowski velocity U_{HS} and the shape factor s on the velocity distribution. It can be concluded from Figure 3 that the profiles are parabolic in nature and the highest velocities are noticed in the middle portion of the peristaltic waves. The velocity reduction is noticed with higher values of the Hartmann number in the middle part of the channel and the trend is reversed near the walls (see Figure 3a). In the presence of a magnetic field, a force called the Lorentz force arises in the flow domain and it leads to a reduction in the fluid flow rate. Moreover, larger velocities are noticed in the absence of the magnetic field. It can be observed in Figure 3b that, with the increasing values of the thermal Grashof number, the velocity of the nanofluid rises near the right wall and reduces near the left wall. It can also be determined that buoyancy forces play a significant role in peristaltic movement. They support the fluid flow along the microchannel. The trend is reversed in case of the Helmholtz–Smoluchowski velocity (see Figure 3c). Figure 3d represents the effects of various nanoparticle shapes, such as bricks, cylinders and platelets, on the velocity profile. It can be seen that the larger velocities are observed in the flow of the nanofluid containing brick-shaped nanoparticles near the right wall, and later the sequence is followed as cylindrical and platelet-shaped nanoparticles, respectively.
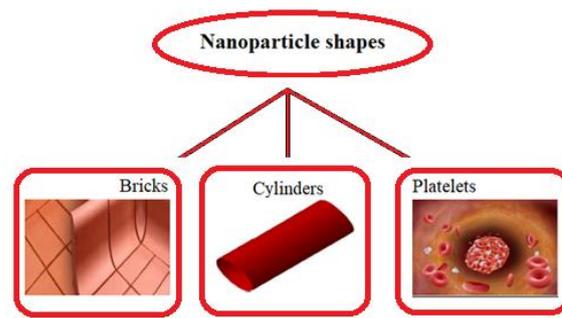
Figure 2. Different nanoparticle shapes.

Table 2. Shape factors and coefficients of the nanoparticles [47,49].

Nanoparticle Shapes	Shape Factor (s)	A_1	A_2
Bricks	3.72	1.9	471.4
Platelets	5.72	37.1	612.6
Cylinders	4.82	13.5	904.4

Figure 4 presents the variations in the temperatures for various values of the radiation parameter Rn, activation energy E, thermophoresis parameter Nt and shape factor s. From the temperature profiles, it can be observed that the structure is likely to be perceived as parabolic in nature. It is clear from Figure 4a that the temperature decreases with the rising values of the radiation parameter. Activation energy increases the temperature (see Figure 4b). A lower thermophoresis parameter produces a lower temperature, and a higher thermophoresis parameter produces a higher temperature (see Figure 4c). Figure 4d depicts the temperature profile for different nanoparticle shapes. It determines that a higher temperature is noticed in the nanofluid flow suspended by brick-shaped nanoparticles and a lower temperature is depicted for platelet-shaped nanoparticles. Figure 5 presents the behavior of the nanoparticle volume fraction with different parameters, for instance, the Brownian motion parameter Nb, activation energy parameter E, radiation parameter Rn and shape factor s. It is clear from Figure 5a that the nanoparticle volume fraction increases with the rising values of the Brownian motion parameter. It can be observed that the nanoparticle volume fraction enhances the activation energy (see Figure 5b). From Figure 5c, it can be observed that as the radiation parameter increases, the nanoparticle volume fraction increases. Figure 5d shows the nanoparticle volume fraction with different nanoparticle shapes in the nanofluid. A lower nanoparticle volume fraction is observed for the nanofluid flow with brick-shaped nanoparticles in the nanofluid, and a higher nanoparticle volume fraction is seen in the case of platelet-shaped nanoparticles in the nanofluid.

Figure 6 is plotted to judge the variation of microorganism concentrations for various parameters, such as activation energy parameter E, temperature ratio parameter β, Peclet number Pe and shape factor s. It is clear from these figures that the behavior of the microorganism concentration is parabolic. From Figure 6a, it can be observed that the motile microorganisms reduce in the channel of the peristalsis with the rising values of the temperature ratio parameter. Activation energy increases the microorganism concentration profile in the peristaltic flow. Microorganism concentration is a decreasing function of the Peclet number (see Figure 6c). In Figure 6d, it can be observed that the platelet-shaped nanoparticles involved in the nanofluid present the highest microorganism concentration, and the brick-shaped nanoparticles involved in the nanofluid present the lowest concentration. Figure 7 presents the effects of the electroosmosis parameter, zeta potential, bioconvection Rayleigh constant and buoyancy ratio constant on the shear stress distribution. Shear stress distribution provides a wave-like form due to peristalsis. It is noted from Figure 7a that the electroosmosis parameter displays the mixed behavior in the channel. Moreover, it is observed from Figure 7b–d that the shear stress increases with the

increasing values of the zeta potential, bioconvection Rayleigh constant and buoyancy ratio constant. The present study is in good agreement with the existing literature by Sridhar and Ramesh [50] (see Figure 8).
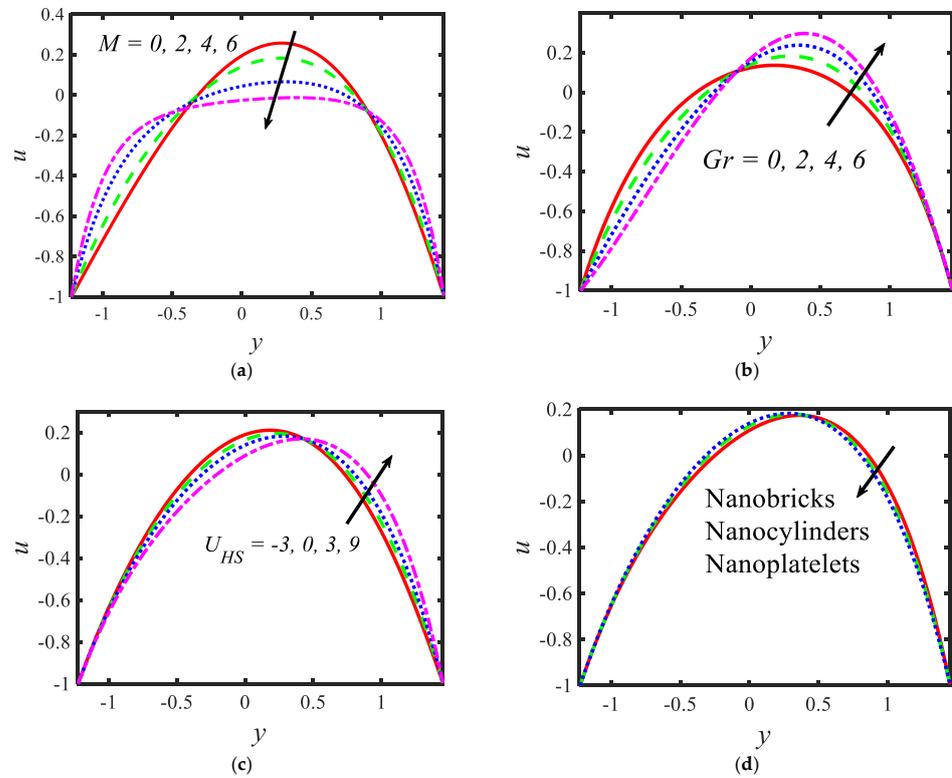
Figure 3. Variations in the velocity profiles for (**a**) the Hartmann number, (**b**) Grashof number, (**c**) Helmholtz–Smoluchowski velocity and (**d**) shape factor.
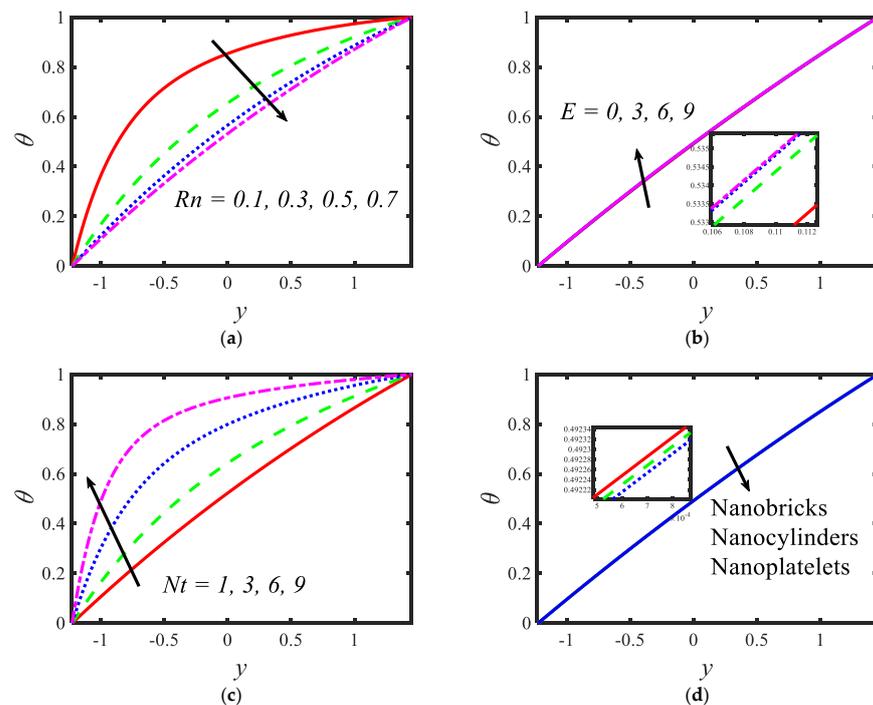
Figure 4. Variations in temperature profiles for (**a**) the radiation parameter, (**b**) Prandtl number, (**c**) thermophoresis parameter and (**d**) shape factor.
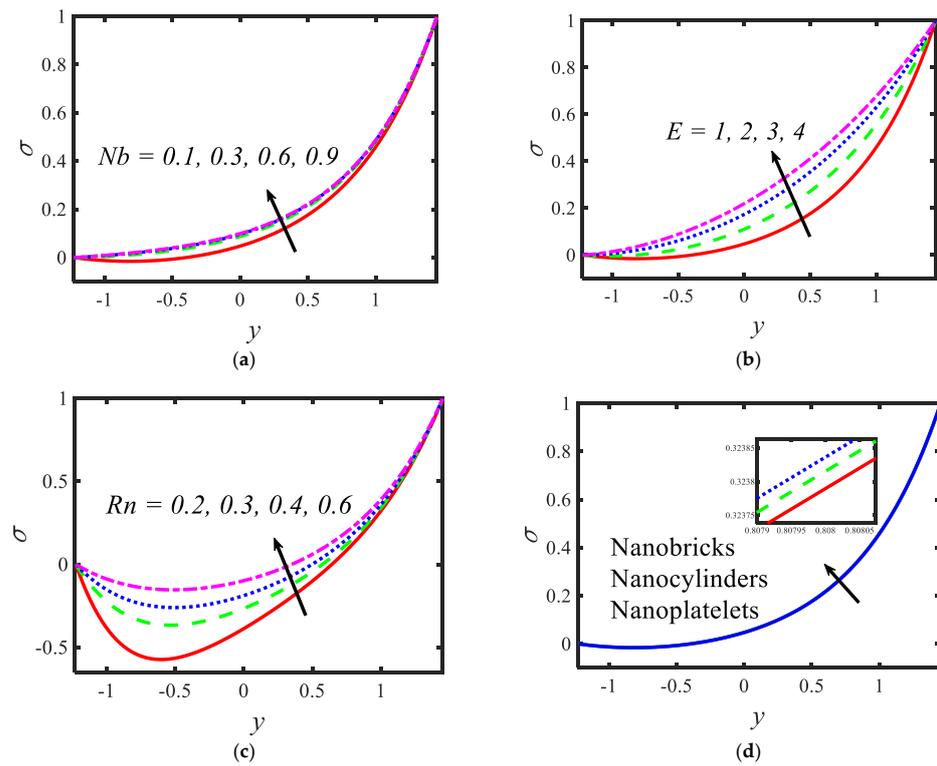
Figure 5. Variations in nanoparticle volume fraction profiles for (**a**) the Brownian motion parameter, (**b**) activation energy parameter, (**c**) radiation parameter and (**d**) the Shape factor.
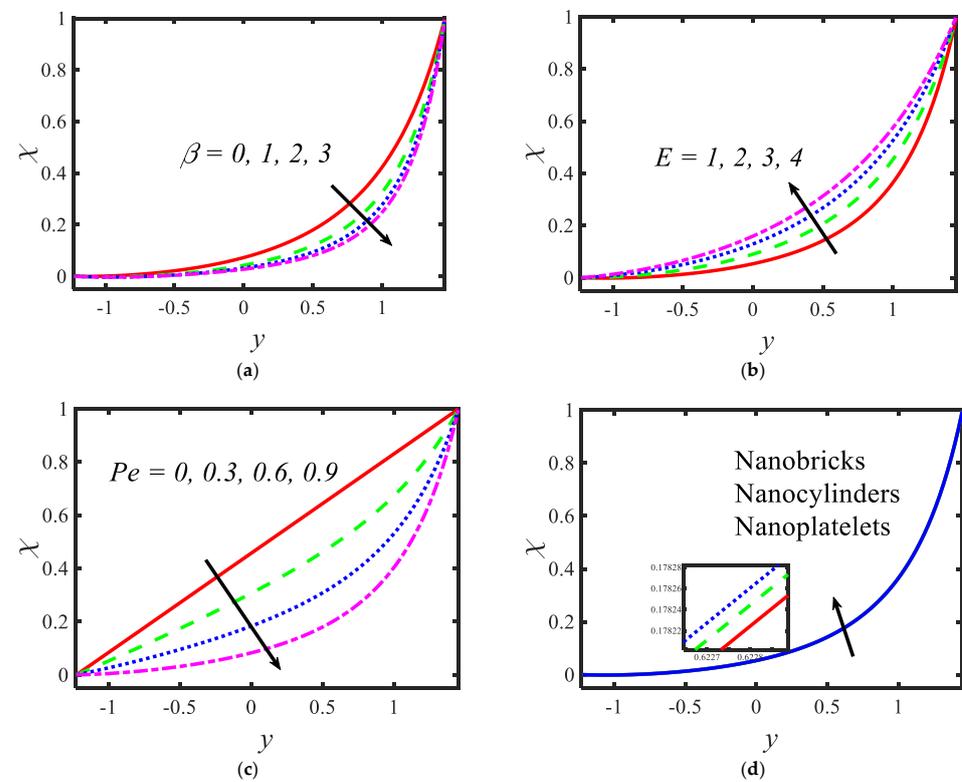
Figure 6. Variations in the motile microorganism profile for (**a**) the temperature ratio parameter, (**b**) activation energy parameter, (**c**) Prandtl number and (**d**) shape factor.
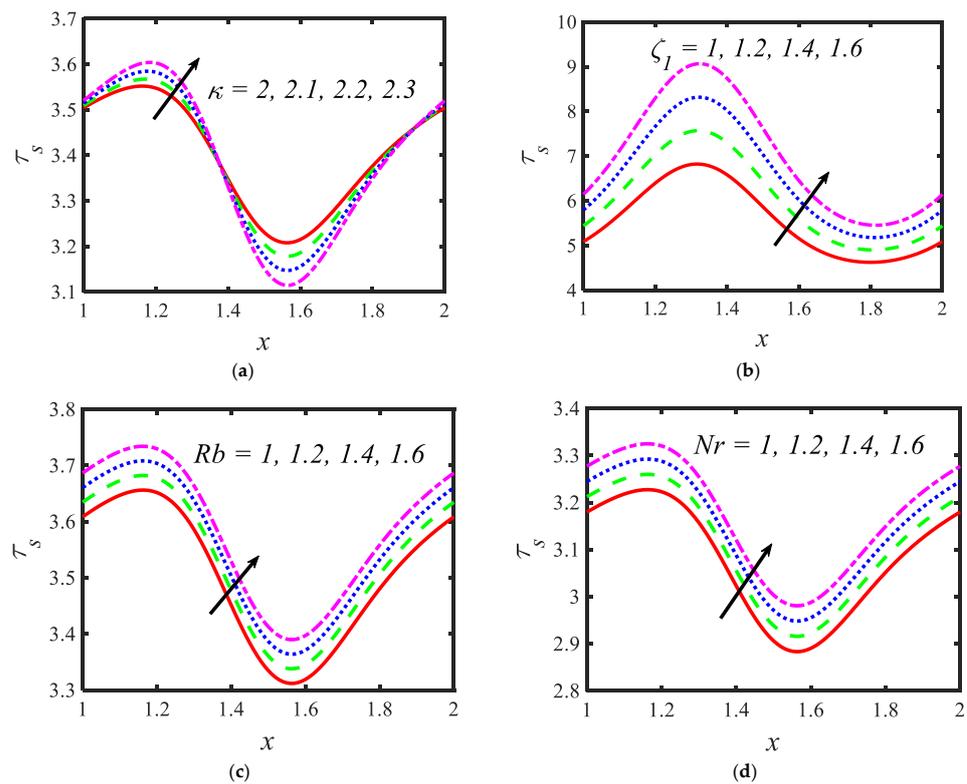
Figure 7. Variations in the shear stress profiles for (**a**) the electroosmosis parameter, (**b**) zeta potential, (**c**) bioconvection Rayleigh constant and (**d**) buoyancy ratio constant.
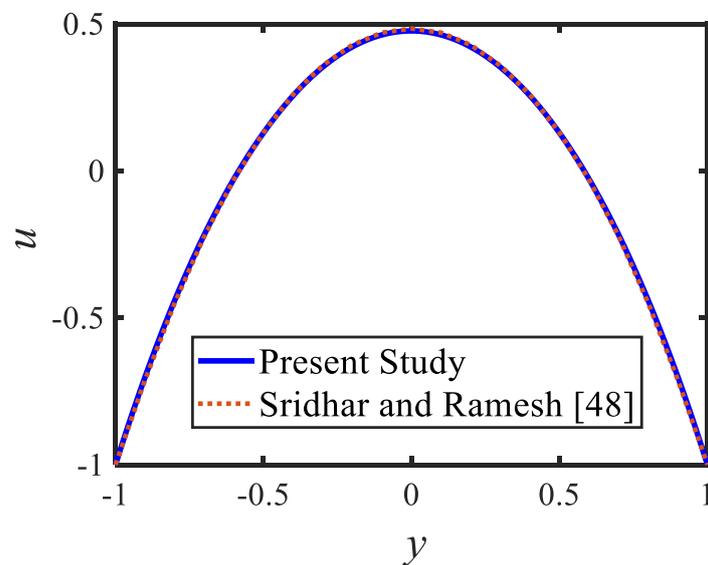
Figure 8. Comparison of the velocity profiles of the present study and [51].

5. Conclusions

In the current article, the influence of activation energy and bioconvection on the propulsion of gold–blood nanofluid is considered in an asymmetric peristaltic channel. The effects of the magnetic field, radiation and electroosmosis were also considered. The system of non-dimensional highly non-linear differential equations were solved by utilizing computational software MATLAB with the help of the bvp4c function. The graphical results were presented for the velocity, temperature, nanoparticle volume fraction, microorganism concentration and shear stress with respect to the sundry parameters. The main findings of the current study are the following:

- The velocity of nanofluid flow suspended by brick-shaped nanoparticles is higher near the right wall, compared with platelet= and cylinder-shaped nanoparticles.
- A higher magnetic field strength suppresses the velocity of the nanofluid.
- Temperature is an increasing function of activation energy and the thermophoresis parameter.
- The radiation parameter reduces the temperature profile.
- The nanoparticle volume fraction increases with the rising values of the Brownian motion parameter and radiation parameter.
- Microorganism concentration increases with the rising values of activation energy.
- Shear stress is an increasing function of zeta potentials and the bioconvection Rayleigh constant.

Author Contributions: Conceptualization, M.A.N. and B.S.; methodology, M.A.N. and B.S.; software, M.A.N. and B.S.; validation, M.A.N. and B.S.; formal analysis, M.A.N. and B.S.; investigation, M.A.N. and B.S.; resources, M.A.N. and B.S.; data curation, M.A.N. and B.S.; writing—original draft preparation, M.A.N. and B.S.; writing—review and editing, M.A.N. and B.S.; visualization, M.A.N. and B.S.; supervision, M.A.N. and B.S.; project administration, B.S.; funding acquisition, M.A.N.; All authors have read and agreed to the published version of the manuscript.

Data Availability Statement: The data that support the findings of this study are available from the corresponding author upon reasonable request.

Conflicts of Interest: The authors declare no conflict of interest.

Nomenclature

(X, Y)	axial and transverse directions of the flow
B_0	uniform magnetic field
T_0	temperature at left wall
C_0	concentration at left wall
N_0	motile organism concentration at left wall
T_1	temperature at right wall
C_1	concentration at right wall
N_1	motile organism concentration at right wall
H_1	left peristaltic wall
H_2	right peristaltic wall
d	width of the channel
a_1	wave amplitude of left wall
a_2	wave amplitude of right wall
λ	wavelength
t	time
c	wave speed
ϕ	phase difference
U, V	velocities in X and Y directions, respectively
ρ_{nf}	nanofluid effective density
μ_{nf}	nanofluid dynamic viscosity
σ_{nf}	nanofluid electrical conductivity
$(\rho\beta)_{nf}$	effective thermal expansion
g	gravitational force
T	nanoparticle temperature
ρ_p	density of nanoparticles ρ_p
ρ_f	density of base fluid
N	motile density

N_0	ambient concentration of motile organisms
γ	volume of microorganisms
ρ_m	motile organism density
ρ_e	electrical charge density
E_x	applied electric field
$(\rho c_p)_{nf}$	effective heat capacity of nanofluid
k_{nf}	thermal diffusivity of nanofluid
σ^*	Stefan–Boltzmann constant
k^*	mean absorption coefficient
D_B	Brownian diffusion coefficient
C	nanoparticle concentration
D_T	thermophoretic diffusion coefficient
T_m	mean temperature
k_r	rate of reaction
n	fitted rate
E_a	activation energy
ω	Boltzmann constant
b^*	chemotaxis constant
W_e	swimming cells speed
P	pressure
ψ	dimensional stream function
F	dimensional constant flow rate
D_m	microorganism diffusion coefficient
θ	nanoparticle temperature
σ	nanoparticle concentration
χ	motile microorganisms
M	Hartmann number
Re	Reynolds number
δ	wave number
Rb	bioconvection Rayleigh constant
Gr	thermal Grashof number
Nr	buoyancy ratio constant
Rn	radiation parameter
τ	effective heat capacity ratio of nanoparticle material-to-liquid heat capacity
Pr	Prandtl number
ξ	reaction rate constant
Sc	Schmidt number
β	temperature ratio parameter
E	activation energy parameter
Nb	Brownian motion parameter
Nt	thermophoresis parameter
Pe	Peclet number
Ω	concentration difference constant for microorganisms
U_{HS}	Helmholtz–Smoluchowski velocity
κ	electroosmosis parameter
ς_1, ς_2	zeta potentials

References

1. Souayeh, B.; Kumar, K.G.; Reddy, M.G.; Rani, S.; Hdhiri, N.; Alfannakh, H.; Rahimi-Gorji, M. Slip flow and radiative heat transfer behavior of Titanium alloy and ferromagnetic nanoparticles along with suspension of dusty fluid. *J. Mol. Liq.* **2019**, *290*, 111223. [CrossRef]
2. Alam, M.W.; Alaaedeen, A.; Souayeh, B.; Essam, Y.; Hdhiri, N.; Hammami, F. Theoretical analysis of carbon nanotubes (SWCNT/MWCNT) over a Wang's stretching sheet under C-C heat flux. *Phys. Scr.* **2020**, *95*, 10. [CrossRef]
3. Souayeh, B.; Hammami, F.; Hdhiri, N.; Alam, M.W.; Yasin, E.; Abuzir, A. Simulation of natural convective heat transfer and entropy generation of nanoparticles around two spheres in horizontal arrangement. *Alex. Eng. J.* **2021**, *60*, 2583–2605. [CrossRef]
4. Ramesh, K.; Reddy, M.G.; Souayeh, B. Electro-Magneto-Hydrodynamic Flow of Couple Stress Nanofluids in Micro-Peristaltic Channel with Slip and Convective Conditions. *Appl. Math. Mech.* **2021**, *42*, 593–606. [CrossRef]

5. Yeh, Y.C.; Creran, B.; Rotello, V.M. Gold nanoparticles: Preparation, properties, and applications in bionanotechnology. *Nanoscale* **2012**, *4*, 1871–1880. [CrossRef] [PubMed]

6. Dykman, L.A.; Khlebtsov, N.G. Gold nanoparticles in biology and medicine: Recent advances and prospects. *Acta Nat.* **2011**, *3*, 34–55. [CrossRef]

7. Elahi, N.; Kamali, M.; Baghersad, M.H. Recent biomedical applications of gold nanoparticles: A review. *Talanta* **2018**, *184*, 537–556. [CrossRef]

8. Daraee, H.; Eatemadi, A.; Abbasi, E.; Aval, S.F.; Kouhi, M.; Akbarzadeh, A. Application of gold nanoparticles in biomedical and drug delivery. *Artif. Cells Nanomed. Biotechnol.* **2016**, *44*, 410–422. [CrossRef] [PubMed]

9. Bansal, S.A.; Kumar, V.; Karimi, J.; Singh, A.P.; Kumar, S. Role of gold nanoparticles in advanced biomedical applications. *Nanoscale Adv.* **2020**, *2*, 3764–3787. [CrossRef]

10. Homberger, M.; Simon, U. On the application potential of gold nanoparticles in nanoelectronics and biomedicine. *Philos. Trans. R. Soc. A Math. Phys. Eng. Sci.* **2010**, *368*, 1405–1453. [CrossRef]

11. Mekheimer, K.; Hasona, W.; Abo-Elkhair, R.; Zaher, A. Peristaltic blood flow with gold nanoparticles as a third grade nanofluid in catheter: Application of cancer therapy. *Phys. Lett. A* **2018**, *382*, 85–93. [CrossRef]

12. Koriko, O.K.; Animasaun, I.; Mahanthesh, B.; Saleem, S.; Sarojamma, G.; Sivaraj, R. Heat transfer in the flow of blood-gold Carreau nanofluid induced by partial slip and buoyancy. *Heat Transf. Asian Res.* **2018**, *47*, 806–823. [CrossRef]

13. Ellahi, R.; Rahman, S.U.; Nadeem, S.; Akbar, N.S. Blood flow of nanofluid through an artery with composite stenosis and permeable walls. *Appl. Nanosci.* **2014**, *4*, 919–926. [CrossRef]

14. Riaz, A.; Gul, A.; Khan, I.; Ramesh, K.; Khan, S.U.; Baleanu, D.; Nisar, K.S. Mathematical analysis of entropy generation in the flow of viscoelastic nanofluid through an annular region of two asymmetric annuli having flexible surfaces. *Coatings* **2020**, *10*, 213. [CrossRef]

15. Elnaqeeb, T.; Shah, N.A.; Mekheimer, K.S. Hemodynamic characteristics of gold nanoparticle blood flow through a tapered stenosed vessel with variable nanofluid viscosity. *BioNanoScience* **2019**, *9*, 245–255. [CrossRef]

16. Frei, E.H. Medical applications of magnetism. *Crit. Rev. Solid State Mater. Sci.* **1970**, *1*, 381–407. [CrossRef]

17. Bahadur, D.; Giri, J. Biomaterials and magnetism. *Sadhana* **2003**, *28*, 639–656. [CrossRef]

18. Roth, B.J. The role of magnetic forces in biology and medicine. *Exp. Biol. Med.* **2011**, *236*, 132–137. [CrossRef] [PubMed]

19. Zablotskii, V.; Polyakova, T.; Lunov, O.; Dejneka, A. How a high-gradient magnetic field could affect cell life. *Sci. Rep.* **2016**, *6*, 37407. [CrossRef]

20. Eldabe, N.T.; Moatimid, G.M.; El-Shekhipy, A.A.; Aballah, N.F. Peristaltic blood flow with gold nanoparticles on a Carreau nanofluid through a non-Darcian porous medium. *J. Biomater. Nanobiotechnol.* **2018**, *9*, 290–306. [CrossRef]

21. Abdelsalam, S.I.; Bhatti, M.M. New insight into AuNP applications in tumour treatment and cosmetics through wavy annuli at the nanoscale. *Sci. Rep.* **2019**, *9*, 260. [CrossRef] [PubMed]

22. Akram, S.; Zafar, M.; Nadeem, S. Peristaltic transport of a Jeffrey fluid with double-diffusive convection in nanofluids in the presence of inclined magnetic field. *Int. J. Geom. Methods Mod. Phys.* **2018**, *15*, 1850181. [CrossRef]

23. El-Dabe, N.T.M.; Abou-Zeid, M.Y.; Mohamed, M.A.A.; Abd-Elmoneim, M.M. MHD peristaltic flow of non-Newtonian power-law nanofluid through a non-Darcy porous medium inside a non-uniform inclined channel. *Arch. Appl. Mech.* **2020**, *91*, 1067–1077. [CrossRef]

24. Devaki, P.; Venkateswarlu, B.; Srinivas, S.; Sreenadh, S. Mhd peristaltic flow of a nanofluid in a constricted artery for different shapes of nanosized particles. *Nonlinear Eng.* **2020**, *9*, 51–59. [CrossRef]

25. Reddy, M.G.; Makinde, O.D. Magnetohydrodynamic peristaltic transport of Jeffrey nanofluid in an asymmetric channel. *J. Mol. Liq.* **2016**, *223*, 1242–1248. [CrossRef]

26. Markov, M.S. (Ed.) *Electromagnetic Fields in Biology and Medicine*; CRC Press: Boca Raton, FL, USA, 2015.

27. Ryan, C.N.M.; Doulgkeroglou, M.N.; Zeugolis, D.I. Electric field stimulation for tissue engineering applications. *BMC Biomed. Eng.* **2021**, *3*, 1. [CrossRef] [PubMed]

28. Cen, C.; Chen, X. The electrode modality development in pulsed electric field treatment facilitates biocellular mechanism study and improves cancer ablation efficacy. *J. Healthc. Eng.* **2017**, *2017*, 1–10. [CrossRef]

29. Roth, B.J.; Hobbie, R.K. A collection of homework problems about the application of electricity and magnetism to medicine and biology. *Am. J. Phys.* **2014**, *82*, 422–427. [CrossRef]

30. Moatimid, G.M.; Mohamed, M.A.; Hassan, M.; El-Dakdoky, E.M.M. Electro-osmotic flow and heat transfer of a non-Newtonian nanofluid under the influence of peristalsis. *Pramana* **2019**, *92*, 90. [CrossRef]

31. Tanveer, A.; Khan, M.; Salahuddin, T.; Malik, M. Numerical simulation of electroosmosis regulated peristaltic transport of Bingham nanofluid. *Comput. Methods Programs Biomed.* **2019**, *180*, 105005. [CrossRef]

32. Sharma, A.; Tripathi, D.; Sharma, R.; Tiwari, A. Analysis of double diffusive convection in electroosmosis regulated peristaltic transport of nanofluids. *Phys. A: Stat. Mech. Appl.* **2019**, *535*, 122148. [CrossRef]

33. Jayavel, P.; Jhorar, R.; Tripathi, D.; Azese, M.N. Electroosmotic flow of pseudoplastic nanoliquids via peristaltic pumping. *J. Braz. Soc. Mech. Sci. Eng.* **2019**, *41*, 61. [CrossRef]

34. Noreen, S.; Waheed, S.; Hussanan, A. Peristaltic motion of MHD nanofluid in an asymmetric micro-channel with Joule heating, wall flexibility and different zeta potential. *Bound. Value Probl.* **2019**, *2019*, 12. [CrossRef]

35. Mekheimer, K.S.; Abo-Elkhair, R.E.; Moawad, A.M.A. Electrothermal transport via gold nanoparticles as antimicrobials of blood flow through an electro-osmosis artery with overlapping stenosis. *Int. J. Fluid Mech. Res.* **2020**, *47*, 135–152. [CrossRef]

36. Khan, I.; Saeed, K.; Khan, I. Nanoparticles: Properties, applications and toxicities. *Arab. J. Chem.* **2019**, *12*, 908–931. [CrossRef]

37. Bharathi, V.; Vijayaragavan, R.; Prakash, J. Comparative analysis of Cu/blood and Cu–CuO/blood nanofluids on a peristaltic flow governed by an asymmetric channel. *Heat Transf.* **2020**, *49*, 4923–4944. [CrossRef]

38. Khan, M.I.; Khan, S.U.; Jameel, M.; Chu, Y.M.; Tlili, I.; Kadry, S. Significance of temperature-dependent viscosity and thermal conductivity of Walter's B nanoliquid when sinusodal wall and motile microorganisms density are significant. *Surf. Interfaces* **2021**, *22*, 100849. [CrossRef]

39. Akbar, N.S. Bioconvection peristaltic flow in an asymmetric channel filled by nanofluid containing gyrotactic microorganism: Bio nano engineering model. *Int. J. Numer. Methods Heat Fluid Flow* **2015**, *25*, 214–224. [CrossRef]

40. Alharbi, F.; Naeem, M.; Zubair, M.; Jawad, M.; Jan, W.; Jan, R. Bioconvection due to gyrotactic microorganisms in couple stress hybrid nanofluid laminar mixed convection incompressible flow with magnetic nanoparticles and chemical reaction as carrier for targeted drug delivery through porous stretching sheet. *Molecules* **2021**, *26*, 3954. [CrossRef]

41. Tripathi, D.; Prakash, J.; Reddy, M.G.; Kumar, R. Numerical study of electroosmosis-induced alterations in peristaltic pumping of couple stress hybrid nanofluids through microchannel. *Indian J. Phys.* **2021**, *95*, 2411–2421. [CrossRef]

42. Tripathi, D.; Prakash, J.; Tiwari, A.K.; Ellahi, R. Thermal, microrotation, electromagnetic field and nanoparticle shape effects on Cu-CuO/blood flow in microvascular vessels. *Microvasc. Res.* **2020**, *132*, 104065. [CrossRef]

43. Bezi, S.; Souayeh, B.; Ben-Cheikh, N.; Ben-Beya, B. Numerical simulation of entropy generation due to unsteady natural convection in a semi-annular enclosure filled with nanofluid. *Int. J. Heat Mass Transf.* **2018**, *124*, 841–859. [CrossRef]

44. Chakraborty, S. Augmentation of peristaltic microflows through electro-osmotic mechanisms. *J. Phys. D Appl. Phys.* **2006**, *39*, 5356. [CrossRef]

45. Tang, G.; Li, X.; He, Y.; Tao, W. Electroosmotic flow of non-Newtonian fluid in microchannels. *J. Non-Newton. Fluid Mech.* **2009**, *157*, 133–137. [CrossRef]

46. Hayat, T.; Rafiq, M.; Ahmad, B.; Asghar, S. Entropy generation analysis for peristaltic flow of nanoparticles in a rotating frame. *Int. J. Heat Mass Transf.* **2017**, *108*, 1775–1786. [CrossRef]

47. Alawi, O.A.; Abdelrazek, A.H.; Aldlemy, M.S.; Ahmed, W.; Hussein, O.A.; Ghafel, S.T.; Khedher, K.M.; Scholz, M.; Yaseen, Z.M. Heat transfer and hydrodynamic properties using different metal-oxide nanostructures in horizontal concentric annular tube: An optimization study. *Nanomaterials* **2021**, *11*, 1979. [CrossRef] [PubMed]

48. Hayat, T.; Abbasi, F.M.; Ahmad, B.; Alsaedi, A. Peristaltic transport of Carreau-Yasuda fluid in a curved channel with slip effects. *PLoS ONE* **2014**, *9*, e95070. [CrossRef] [PubMed]

49. Iqbal, Z.; Akbar, N.S.; Azhar, E.; Maraj, E.N. Performance of hybrid nanofluid (Cu-CuO/water) on MHD rotating transport in oscillating vertical channel inspired by Hall current and thermal radiation. *Alex. Eng. J.* **2018**, *57*, 1943–1954. [CrossRef]

50. Sridhar, V.; Ramesh, K. Entropy generation analysis on EMHD peristaltic propulsion of blood-mediated gold-silver nanoparticles: Application to fatal diseases. *Waves Random Complex Media* **2022**, *2022*, 1–26. [CrossRef]

51. Javed, T.; Hamid, A.H.; Ahmed, B.; Ali, N. Effect of heat transfer on peristaltic flow in presence of heat generation against higher value of Reynolds number using FEM. *J. Theor. Appl. Mech.* **2021**, *59*, 279–292. [CrossRef]